In: Modeling Hydrologic Effects …
Editor: Xixi Wang, pp. 33-58
ISBN 978-1-61668-628-4

Chapter 3

NUMERICAL MODELING OF TRANSPORT PROCESSES AT HILLSLOPE SCALE ACCOUNTING FOR LOCAL PHYSICAL FEATURES

Gokmen Tayfur*
[1]Department of Civil Engineering, Izmir Institute of Technology,
Gulbahce Kampus, Urla, Izmir 35430, Turkey

ABSTRACT

Hillslope is the basic unit of a watershed. Typical hillslopes may have a size of 1000 m long and 500 m wide. For watershed modeling, it is essential to accurately describe the hillslope-scale processes of flow, erosion and sediment transport, and solute transport. Although these processes are usually considered in experimental studies and theoretical subjects, the existing numerical models that are designed to simulate transport processes at hillslope scale rarely take microtopographic variations into account. Instead, those models assume constant slope, roughness, and infiltration rate for a given basic computational unit (i.e., hillslope). As a result, effects of microtopographic features (e.g., rills) on the aforementioned processes cannot be reflected in modeling results. However, the effects could be important because rill and sheet flows exhibit distinctly different dynamics that influence the transport processes. The objective of this chapter is to review the numerical studies for investigating the transport processes at hillslope scale. The chapter focuses particularly on the modeling efforts with the effects of microtopographic features on the dynamics of the transport processes incorporated.

Keywords: Hillslope, flow, sediment, simulation, microtopography, rill, interrill, roughness, infiltration

* E-mail: gokmentayfur@iyte.edu.tr

INTRODUCTION

In the past decades, variety of models have been developed to simulate hydrologic and hydraulic processes in watersheds with a size of thousands of square kilometers (e.g.,the Euphrates river basin in Turkey). These models are usually used for: 1) planning, design, and operation of projects to conserve water and soil resources and to protect their quality (e.g., planning and designing soil conservation practices, irrigation water management, wetland restoration, stream restoration, and water-table management, flood protection projects, rehabilitation of aging dams, floodplain management, water-quality evaluation, and water supply forecasting); 2) water resources assessment, development, and management (e.g., analyzing the quantity and quality of streamflow, reservoir system operations, groundwater development and protection, surface water and groundwater conjunctive use management, water distribution systems, and water use); 3) assessing impacts of climate change on national water resources and agricultural productivity; and 4) quantifying impacts of watershed management strategies on environmental and water resources protection (Wurbs 1998; Mankin et al. 1999; Rudra et al. 1999; Singh and Woolhiser 2002).

The use of these watershed models can be greatly facilitated with the available data on topography, soil, land use, and hydrography (Engman and Gurney 1991). For example, digital imagery provides mapping of spatially varying landscape attributes, while radar is being employed for rainfall measurements. Digital elevation models (DEMs), with a typical resolution of 30 m by 30 m, can be used to derive basin geometry, stream networks, slope, aspect, flow direction (Singh and Woolhiser 2002). The use of a geographic information system (GIS) facilitates the: 1) subdivision of a watershed into hydrologically homogeneous subareas in both horizontal and vertical domains; 2) determination of soil loss rates; 3) identification of potential areas of nonpoint source contaminants; 4) maping of groundwater contamination susceptibility; and 5) incorporation of spatial details beyond the existing capability of watershed hydrologic models (Singh and Woolhiser 2002).

Hillsopes form subsections within a watershed. The sizes of the subsections can range from 100 to 500,000 m^2, and a hillslope usually includes one computational cell or more, depending on the cell size. For example, a 900 m by 90 m hillslope consists of 90 numerical computational cells with a size of 30 m by 30 m. As a result, a small size hillslope may form one single computational cell of a watershed, but a large size hillslope would constitute hundreds computational cells. Thus, the dynamics of hydrologic processes at the hillslope scale can greatly influence the ones of hydrologic processes at the watershed scale. The accurate description of the hillslope-scale dynamics is very important for watershed modeling and analysis.

Conventionally, numerical models for transport processes over hillslope assume a smooth surface and do not consider the microtopographic variations on the surface. One justification for this simplification is that considering microtopography could noticeably increase the complexity of the numerical procedure and mandate extra efforts to obtain high-resolution microtopographic data. Zhang and Cundy (1989) and Tayfur et al. (1993) qualitatively investigated the flow over varying microtopographic surfaces at the hillslope scale. In a separate study, Tayfur and Singh (2004) modeled sediment transport over microtopographic surfaces. These studies revealed the importance of varying the infiltration rate, roughness, and local slope, for the analysis of hillslope hydrologic dynamics.

Land surfaces, on which transport processes occur, contain irregular microtopography and/or rills. Transport over such surfaces occurs in both rill and interrill areas (Figure 3-1). Runoff over hillslopes or agricultural watersheds initially starts as sheet flow, and then it concentrates into a series of small channels. The flow concentrations depend on either topographic irregularities or differences in soil erodibility or both. As runoff continues and the erosion progresses, these channels are deepen and widen as a function of slope steepness, runoff characteristics, and soil erodibility. Such erosion-formed microchannels are defined as rills (Emmett 1978; Li et al. 1980). The importance of rills on flow dynamics and sediment transport has been well observed in field and laboratory experimental studies. For example, Meyer et al. (1975) studied the influence of rilling in determining the source of eroded soil in agricultural plots, and observed that there was a significant increase in sediment loss due to the presence of rills. They found that the transport capacity of the rill flow is much greater than that of sheet flow over interrill areas; soil loss increases three to five times when rill develops on a surface. These results were verified in subsequent independent experiemental studies (e.g., Moss and Walker 1978; Abrahams et al. 1989; Abrahams and Parsons 1990; Govindaraju and Kavvas 1992). In addition, Kavvas and Govindaraju (1992) and Tayfur and Kavvas (1994; and 1998) investigated numerical modeling flow over rilled-surfaces employing physically-based flow equations. Tayfur (2007) investigated erosion and sediment transport from rilled surfaces using physically-based erosion and sediment transport equations. These three studies indicate that rills have a significant effect on the transport processes.

These experimental results provide a good opportunity to improve the existing numerical models to reflect the differences in transport capacities of rills and their adjunct interrills. The purpose of this chapter is to review the numerical modeling efforts for simulating transport of flow and sediment through hillslopes, which take into account effects of local features (e.g., microtopographic rills).

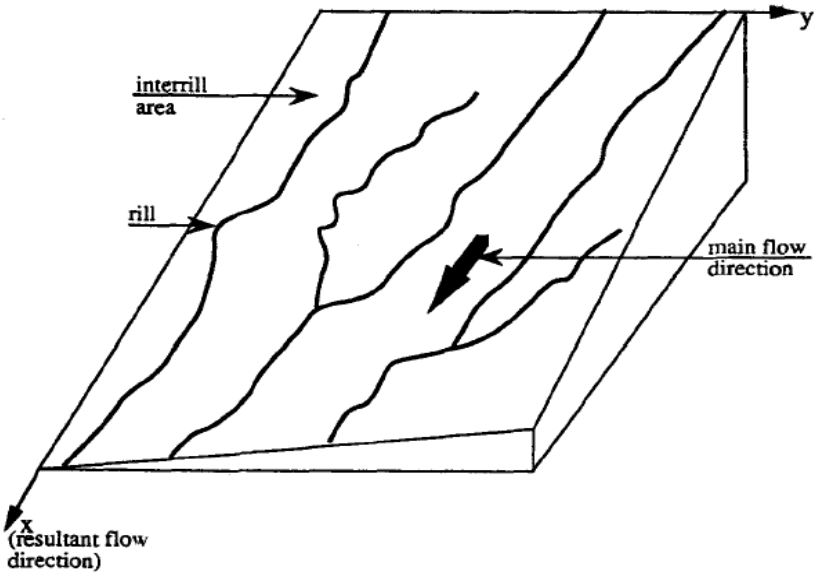

Figure 3-1. Schematic of a hillslope with rills and interrills.

MODELING OVERLAND FLOW OVER MICROTOPOGRAPHIC SURFACE

Overland flows may cause surface erosion and result in flash response in the stream hydrograph. The hydraulics of overland flows is very important in determining flow depth, velocity, and its transport capacity of sediment and chemicals (Moore and Foster 1989). In addition, overland flows can carry nonpoint source pollutants from agricultural lands into receiving water bodies (e.g., channels, natural lakes, and reservoirs). Although numerical techniques (e.g., finite difference, finite volume, or finite element) are effective to solve the governing equations, the direction solution to the St. Venant equations can incur problems of instability and divergence because of the highly nonlinear nature of these equations. Alternatively, researchers simplify the St. Venant equations by only considering important hydraulic processes for the purpose of solving practical problems, resulting in the commonly used kinematic and diffusion wave models.

The two-dimensional St.Venant equations can be expressed as (Tayfur et al. 1993):

$$\frac{\partial h}{\partial t}+\frac{\partial (hu)}{\partial x}+\frac{\partial (hv)}{\partial y}= [r-i] \tag{1}$$

$$\frac{\partial u}{\partial t}+u\frac{\partial u}{\partial x}+v\frac{\partial u}{\partial y}+g\frac{\partial h}{\partial x}= g\left[S_{ox}-S_{fx}\right] \tag{2}$$

$$\frac{\partial v}{\partial t}+u\frac{\partial v}{\partial x}+v\frac{\partial v}{\partial y}+g\frac{\partial h}{\partial y}= g\left[S_{oy}-S_{fy}\right] \tag{3}$$

where h is the flow depth; u and v are the depth-averaged flow velocities in x- and y-directions, respectively; r is the rainfall intensity; i is the infiltration rate; S_{ox} and S_{oy} are the bed slopes in x- and y- directions, respectively; g is the gravitational acceleration; and S_{fx} and S_{fy} are the friction slopes in x- and y- directions, respectively, which can be computed using Manning's equation expressed as:

$$S_{fx}=\frac{n^2 u\sqrt{u^2+v^2}}{h^{4/3}} \tag{4a}$$

$$S_{fy}=\frac{n^2 v\sqrt{u^2+v^2}}{h^{4/3}} \tag{4b}$$

where n is the Manning's roughness coefficient.

The diffusion wave model neglects the local inertia terms (i.e., the second and third terms in Eqs. 2 and 3), whereas, the kinematic model neglects the first three terms in Eqs. (2) and (3). Zhang and Cundy (1989) investigated effects of varying slope, roughness, and infiltration rate on predicting flows over an artificial domain. Tayfur et al. (1993) used the St. Venant equations as well as the kinematic and diffusion wave models to route flow over an

experimental plot (Figure 3-2), and compared the numerical results with the observed hydrographs (Figs. 3, 4, 5, and 6). The plot has average slopes in y- and x-directions of 8.6 and 0.86%, respectively, but the local slopes were computed to be as steep as 15% for the 0.6-m grid resolution. The depressions and crests on the surface may form nodal locations with steep negative slopes, function as storages, and have backwater effects. These physical situations invalidate the kinematic wave model because it assumes that the characteristics move in the forward direction only. The numerical solutions of the St. Venant equations and the diffusion wave model failed to converge even with very small time steps because of the rapidly changing flow regime. The regime of flow with highly variable microtopography is very different from that of sheet flow as assumed by the St. Venant equations. In order to stabilize the solutions, the authors smoothed the surface to obtain a more gradually varying topographic profile. In the flow direction, the local slopes were averaged/smoothed within a 0.6-m window. In contrast, because the local slopes have abrupt changes in the transverse direction, the slopes were averaged within a 1.2-m window to get consistent numerical results. Thus, while the numerical procedure requires a very fine grid resolution to achieve sufficient computational accuracy, the tiny topographic variations have to be smoothed out to satisfy the gradually varying assumption of the St. Venant flow equations.

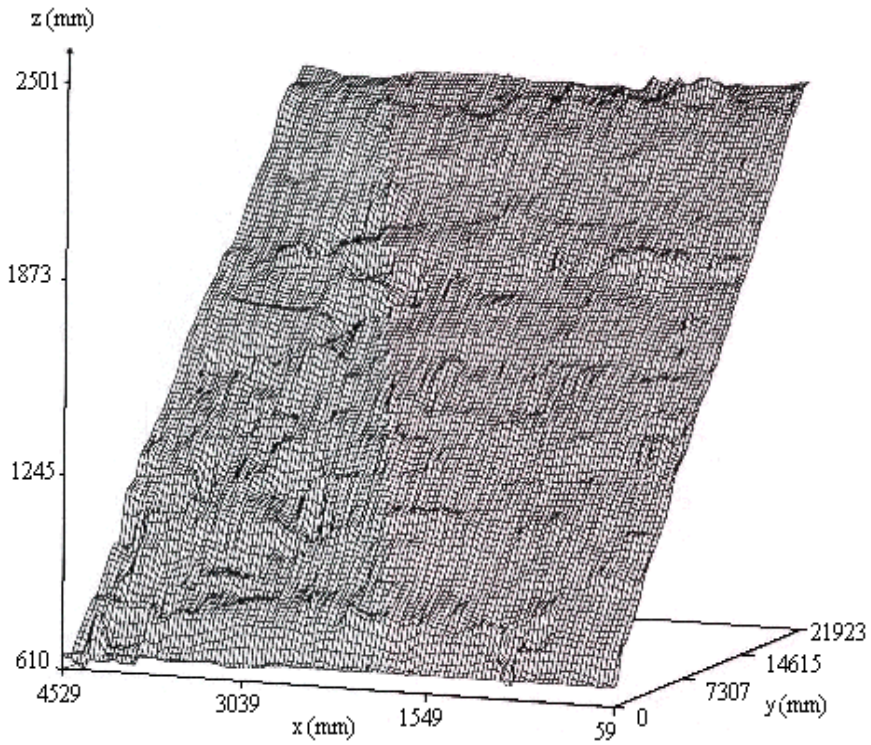

Figure 3-2. The mircotopography of the study plot S3R2A. (Barfield, B.J. and Storm, D.E., Department of Agricultural Engineering at University of Kentucky, Lexington, Kentucky, USA, personal communications, 1989).

The results indicate that there are negligible differences between flow hydrographs predicted using the average slope (Figure 3-3) and those predicted using varying slopes (Figure 3-4). This is probably because the smoothing process removed the partial storage and backwater effects of the microtopographic features, as indicated by the near-identical rising limbs of the hydrographs shown in Figs. 3-3 and 3-4.

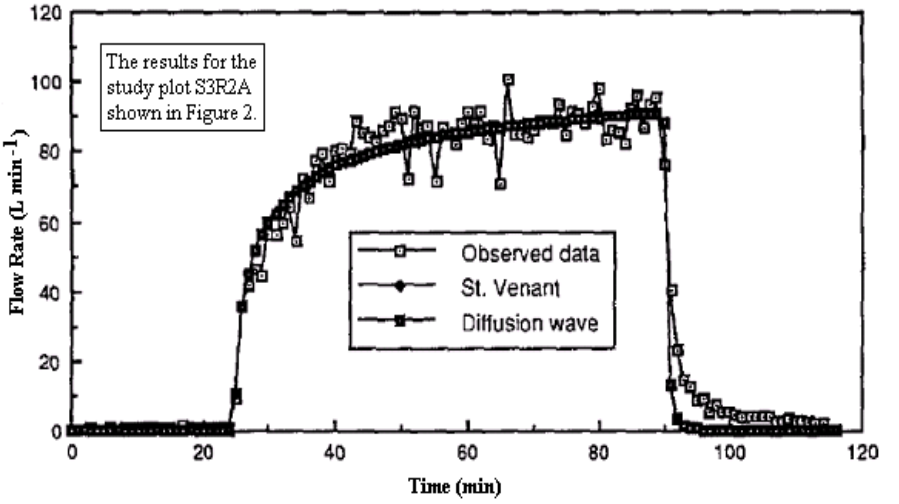

Figure 3-3.The observed versus simulated flow hydrographs using the average slope. (After Tayfur et al. 1993).

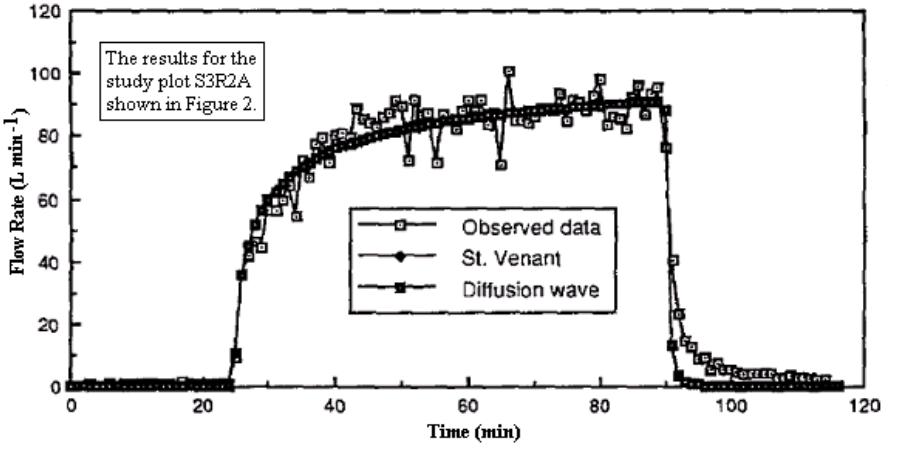

Figure 3-4.The observed versus simulated flow hydrographs using variable slopes. (After Tayfur et al. 1993).

However, the smoothing process did not remove influences of the microtopography on predicting the spatial variations of the local flow depths (Figure 3-5a versus Figure 3-5b) and velocities (Figure 3-6a versus Figure 3-6b), as indicated by the distinctly different predicted spatial patterns. These differences reflect the effects of the microtopographic features. While there is a gradual increase in the flow depth with increasing distance downstream in the *x*- and *y*-directions, the increase pattern is not smooth. The velocities predicted using the average

slope exhibit a gradual variation both in magnitude and direction (Figure 3-6a), which is different from the pattern of the velocities predicted using variable slopes (Figure 3-6b). When the microtopography is considered, the predicted velocity magnitude gradually increases with slope length, but the velocity direction show great deviations from this pattern at the upstream end of the hillslope, where the water depth is shallow. The variations tend to become smaller as the increase of water depth towards the downstream.

MODELING OVERLAND FLOW OVER RILLED SURFACE

In order to study dynamics of flow over rilled surface, Tayfur and Kavvas (1994; 1998) developed a physically-based model. The model simulates overland flows by combining dynamics of rill flow with those of interrill sheet flow at hillslope scale. The model assumes the interrill sheet flow to be two-dimensional and considers the natural variability of microtopography. On the other hand, the model treats the rill flow to be one-dimensional. A rill receives lateral flows from its adjunct interrill areas, with no reverse flows (Figure 3-7).

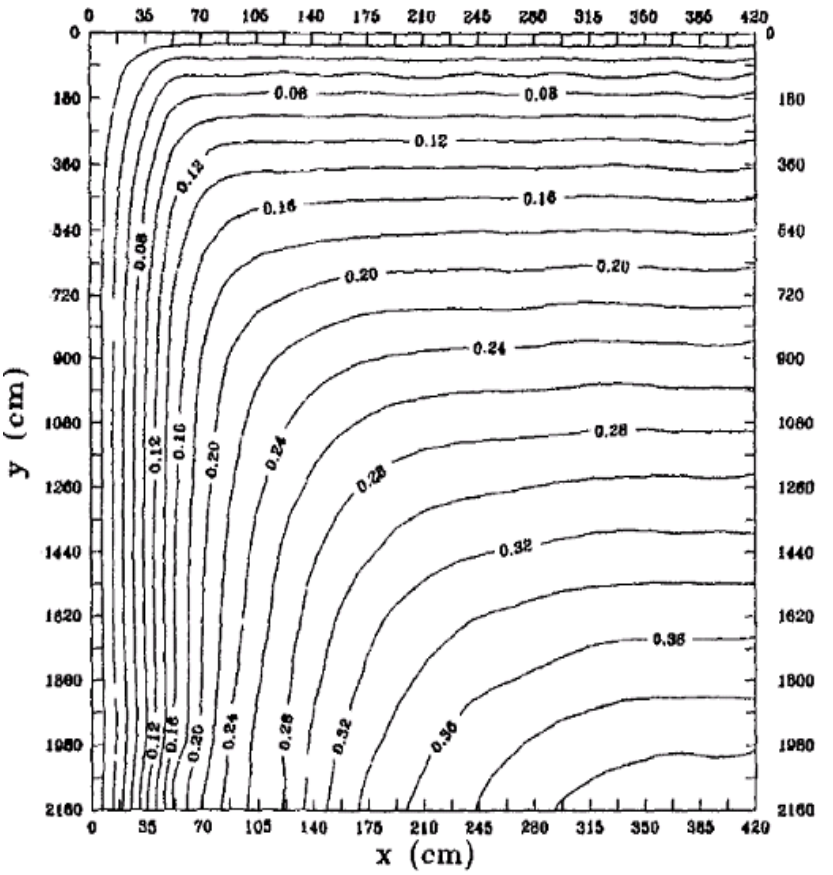

(a)

Figure 3-5. (Continued)

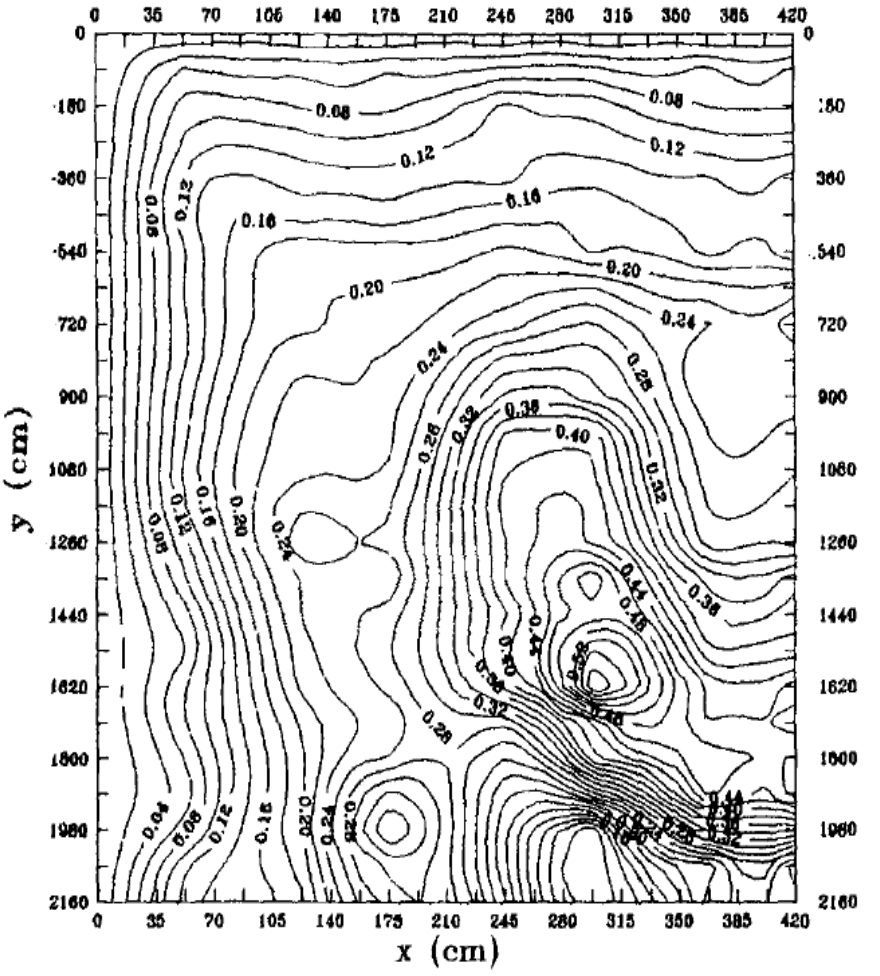

(b)

Figure 3-5. Contour maps pf the overland flow depth, in cm, predicted using (a) the average slope and (b) variable slopes smoothed within a 1.2-m by 0.6-m window. (After Tayfur et al 1993).

For an infinitesimal interrill area, the two-dimensional sheet flow can be approximated by the kinematic wave locally and described by a one-dimensional interrill sheet flow equation (Tayfur and Kavvas 1994). The equation uses the flow averaged over the width of the interrill area (Figure 3-8; Tayfur and Kavvas 1994), and is expressed as:

$$\frac{\partial \bar{h}_o}{\partial t} + \frac{\partial}{\partial x}\left(K'_x \bar{h}_o^{3/2}\right) = \bar{q}_l - 1.97\frac{K_y}{l}\bar{h}_o^{3/2} \qquad (5)$$

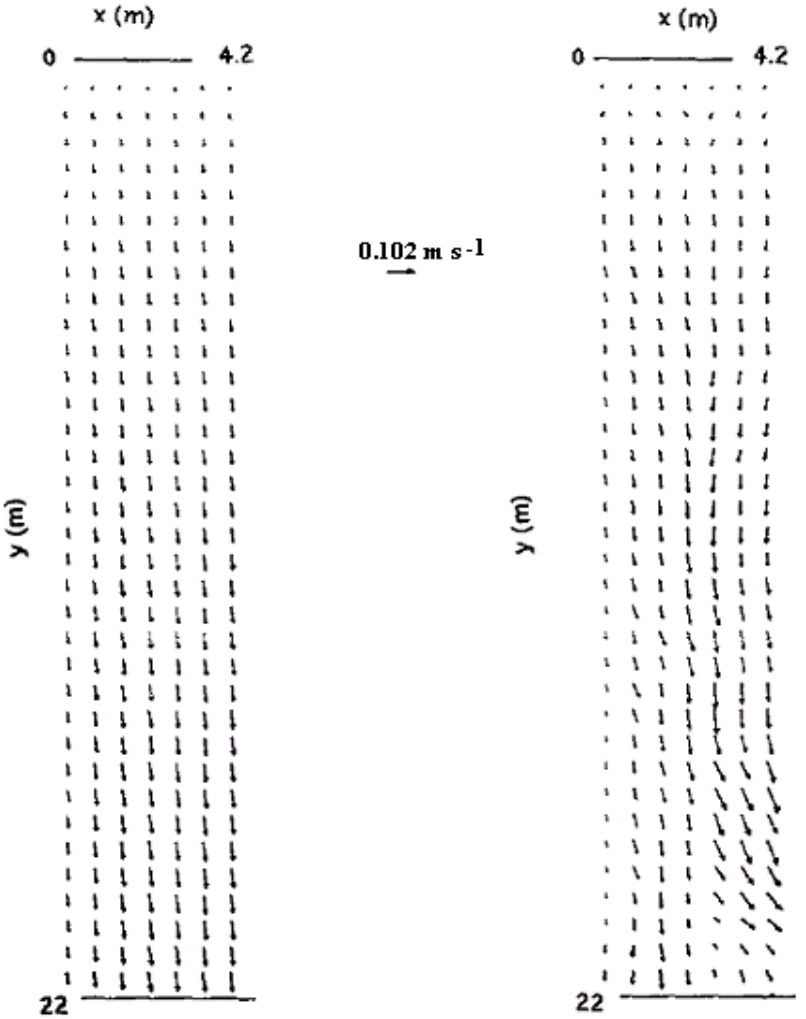

Figure 3-6. The flow velocities predicted using (a) the average slope and (b) variable slopes. (After Tayfur et al. 1993).

where $\overline{h}_o$ is the averaged interrill sheet flow depth; $\overline{q}_l$ is the averaged net lateral flow (i.e., the difference between rainfall and infiltration); K'_x is the expected value of K_x over the interrill area (Figure 3-8).

K_x and K_y are defined as:

$$K_x = \frac{C_z S_{ox}^{0.5}}{\left[1+\left(\frac{S_{oy}}{S_{ox}}\right)^2\right]^{1/4}} \tag{6a}$$

$$K_y = \frac{C_z S_{oy}^{0.5}}{\left[1+\left(\frac{S_{ox}}{S_{oy}}\right)^2\right]^{1/4}} \tag{6b}$$

where C_z is the Chezy roughness coefficient.

The advantage gained by this averaging is that it is not necessary to solve the flow in two dimensions so that there is no need for a finite-difference mesh. This local averaging explicitly yieldes the term representing the water flux from interrill areas into rills, which is represented by the last term on the right hand side of Eq (5). This averaging approach is extended to transects of a hillslope along the orthogonal direction to the main resultant flow (Tayfur and Kavvas 1994) to derive an equation that combines rill flow and interrill sheet flow at the scale of the hillsope transect (Figure 3-8). This equation does not separately model flows in each rill and over each interrill area because the model parameters are individually computed for each hillslope transect.

However, because this model routes flows from transect to transect, it requires detailed geometric data of interrill areas and rills (Tayfur and Kavvas 1994). Thus, applications of this model may be limited by the data availability and computational complexity. To overcome this shortcoming, Tayfur and Kavvas (1998) suggested to integrate Eq. (5) over the hillslope length and to approximate rill flows using an one-dimensional rectangular channel flow (Figs. 9 and 10) equation expressed as:

$$\frac{\partial h_r}{\partial t} + \frac{\partial}{\partial x}\left(K_r \frac{w_r^{0.5} h_r^{1.5}}{\left[w_r + 2h_r\right]^{0.5}}\right) = q_l + 1.97 \bar{h}_o^{3/2}\left(\frac{K_{y1}}{w_r} + \frac{K_{y2}}{w_r}\right) \tag{7}$$

where h_r is the cross-sectionally averaged rill flow depth; w_r is the rill width; $K_r = C_{zr}\sqrt{S_{rx}}$; S_{rx} is the rill bed slope; and C_{zr} is the Chezy roughness coefficient for rill sections; and K_{y1} and K_{y2} are computed using Eq. (6b) for the local interrill area 1 and the local interrill area 2 illustrated in Figure 3-7.

Eq. (7) assumes that flows in the rill and over the adjunct interrill areas follow a sine profile and that the rill width at a given location does not change with time. It also assumes that there is no overflow from the rill to the interrill areas. The locally areal-averaged interrill sheet flow and rill flow equations are expressed as (Tayfur and Kavvas 1998):

$$\frac{\partial \hat{h}_o}{\partial t} + \frac{1.97}{L_x}\left(\hat{K}_{xL_x} \hat{h}_o^{3/2}\right) = \hat{q}_l - 3.88 \hat{K}_{yl} \hat{h}_o^{3/2} \tag{8}$$

$$\frac{\partial \hat{h}_r}{\partial t} + \left(\frac{1.97 K_R \hat{h}_r^{1.5}}{\left[w_{rL_x} + \pi \hat{h}_r\right]^{0.5}}\right) = \hat{q}_l + 3.88 \hat{h}_o^{3/2}\left(\hat{K}_{Y_1} + \hat{K}_{Y_2}\right) \tag{9}$$

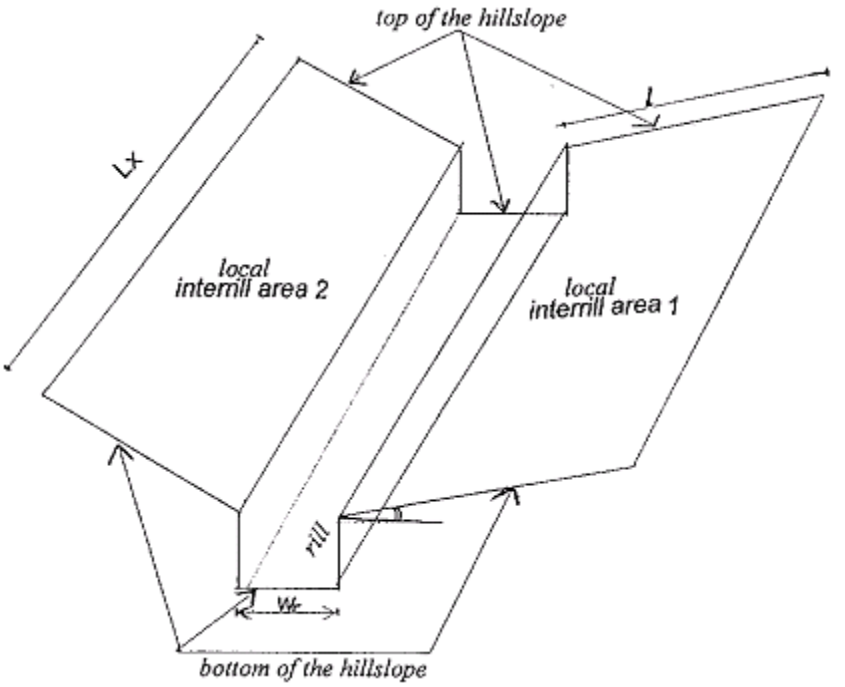

Figure 3-7. The conceptualization of a rill and its adjunct interrill areas.

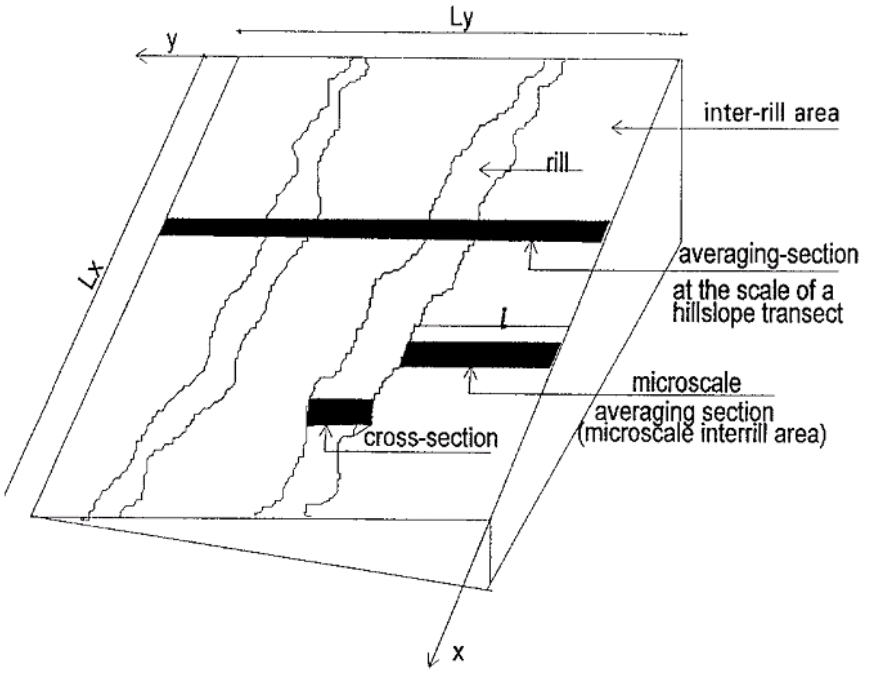

Figure 3-8. Schematic of the averaging section of hillslope.

where $\hat{h}_o$ and $\hat{h}_r$ are the areal-averaged flow depths over the interrill area and in the rill, respectively; $\hat{q}_l$ is the areal-averaged net lateral flow; $K_{yl} = K_y/l$; and $\hat{K}_{XL_x}$ is the interrill areal-averaged K_x at the hillslope bottom; $K_R = \dfrac{K_{rLx} w_{rLx}}{Lx}$ and $K_{Yi} = \dfrac{K_{yi}}{w_r}$, $i = 1,2$; K_{rLx} = K_r as determined for the bottom of the hillslope; and w_{rLx} is the rill width at the bottom of the hillslope.

Eq. (8) is for modeling flow of an individual interrill area section (Fig.3-9), whereas, Eq. (9) is for modeling flows of an individual rill section (Fig.3-9). However, given the large number of rill and interrill sections for a hilllsope, it may be ineffective to solve the dynamics section by section. Instead, Tayfur and Kavvas (1998) suggested to statistically aggregate Eqs. (8) and (9) over a whole hilllsope section (Fig.3-10) using the regular perturbation method that considers the first two terms of a Taylor series expansion. The method assumes that the randomness of variables is solely inherited from the physical model. The aggregated equation for an interrill section is expressed as:

$$\frac{\partial h_o'(\bar{r}')}{\partial t} + 0.985\sum_{i=1}^{n}\sum_{j=1}^{n} Cov(r_i, r_j)\left\{\frac{\partial^2\left[K_X'(\bar{r}')h_o'^{1.5}(\bar{r}')\right]}{\partial r_i' \partial r_j'} + 1.97\frac{\partial^2\left[K_{yl}'(\bar{r}')h_o'^{1.5}(\bar{r}')\right]}{\partial r_i' \partial r_j'}\right\} \tag{10}$$
$$+ 1.97\left\{K_X'(\bar{r}')h_o'^{1.5}(\bar{r}') + 1.97K_{yl}'(\bar{r}')h_o'^{1.5}(\bar{r}')\right\} = \langle q_l' \rangle$$

The aggregated equation for a rill section is expressed as:

$$\frac{\partial h_r'(\bar{r}')}{\partial t} + 0.985\sum_{i=1}^{n}\sum_{j=1}^{n} Cov(r_i, r_j)\left\{\frac{\partial^2\left[\dfrac{K_R(\bar{r}')\ h_r'^{1.5}(\bar{r}')}{\left(w_{r_{Lx}} + \pi h_r'(\bar{r}')\right)^{0.5}}\right]}{\partial r_i' \partial r_j'} - \right.$$
$$\left. 1.97\frac{\partial^2\left[K_{Y_1}'(\bar{r}')\ h_o'^{1.5}(\bar{r}')\right]}{\partial r_i' \partial r_j'} - 1.97\frac{\partial^2\left[K_{Y_2}'(\bar{r}')\ h_o'^{1.5}(\bar{r}')\right]}{\partial r_i' \partial r_j'}\right\} \tag{11}$$
$$1.97\left\{\frac{K_R(\bar{r}')\ h_r'^{1.5}(\bar{r}')}{\left[w_{r_{Lx}} + \pi h_r'(\bar{r}')\right]^{0.5}} - 1.97\ h_o'^{1.5}(\bar{r}')\left[K_{Y_1}'(\bar{r}') + K_{Y_2}'(\bar{r}')\right]\right\} = \langle q' \rangle$$

where $h_o'(\bar{r}')$ and $h_r'(\bar{r}')$ are the hillslope areal-averaged interrill sheet flow and rill flow depths, respectively; and $\bar{r}'$ is the mean vector of the hillslope vector random variable $\bar{r}$ = *(C_z, S_{ox}, S_{oy}, S_r, w_r, l, L_x)*.

To obtain the complete solution to overland flow at the scale of a hillslope, the large-scale areal-averaged interrill sheet flow Eq. (10) and the large-scale areal-averaged rill flow Eq. (11) are solved conjunctively. Eq.(10) is solved first to obtain the areal-averaged discharge flowing into a rill from its adjunct interrill areas as well as the areal-averaged discharge into the stream at the hillslope bottom. Sequentially, Eq. (11) is solved to calculate the areal-averaged discharge from a rill to the stream. The total discharge into the stream is

the summation of the discharges from all rills of the hillslope after corrected by considering a probability of rill occurrence λ (Govindaraju and Kavvas 1992; Kavvas and Govindaraju 1992). The large-scale areal-averaged rill flow discharge to the stream is multiplied by λ, while the large-scale areal-averaged interrill sheet flow discharge to the stream is multiplied by (1-λ). These productions are summed up to determine the total discharge into the stream.

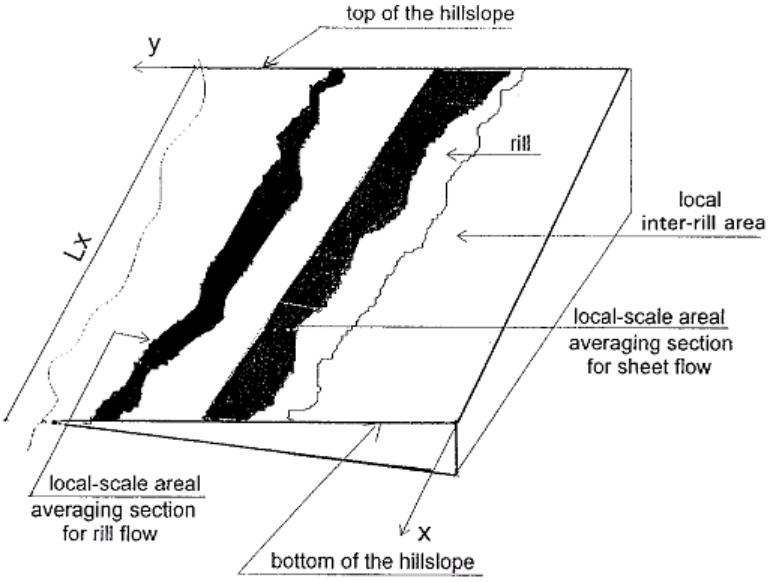

Figure 3-9. Schematic of a local-scale areal averaging section.

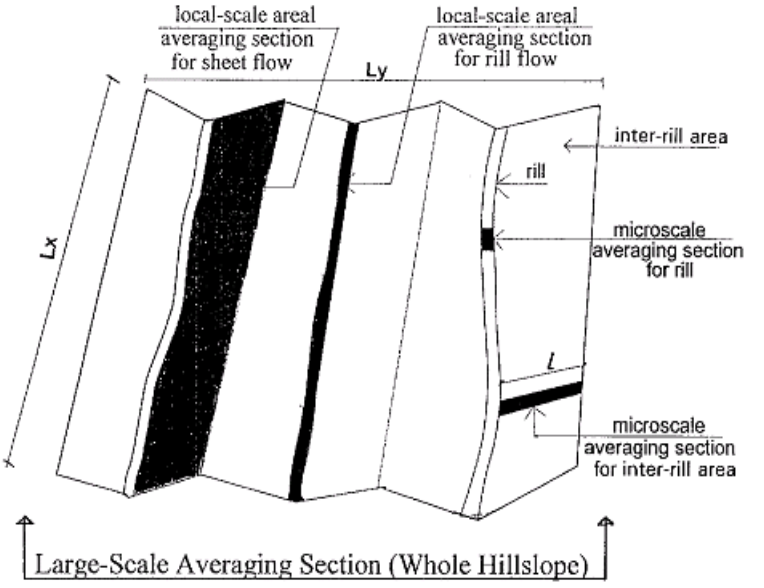

Figure 3-10. Schematic of a hillslope-scale averaging section.

Table 3-1. Summary of the inputs into the model as defined by Eqs. (10) and (11)[1]

Variable	Value	Variable	Value	Variable	Value
L_x (m)	22	S_{oy} (%)	5.2	Cov (S_{ox}, S_{oy})[2]	1.02×10^{-3}
L_y (m)	4.2	l (m)	0.31	Cov (S_{ox}, S_{oy})[2]	0.0041
Rill Number	6	w_r (m)	0.10	C_h (cm hr^{-1})	0.65
R (mm hr^{-1})	97	λ (%)	13.8	p	0.42
t_r (min)	90	Var (S_{ox})[2]	3.24×10^{-4}	Ψ (cm)	18
t_p (min)	20	Var (S_{oy})[2]	0.00112		
S_{ox} (%)	9.1	Var (L_y)[2]	0.095		

r is rainfall intensity; t_r is rainfall duration; t_p is ponding time; C_h is saturated hydraulic conductivity; p is available porosity; Ψ is wetting front capillary pressured head. The other variables are defined in Eqs. (10) and (11). Var ( ) is variance and Cov ( ) is covariance.

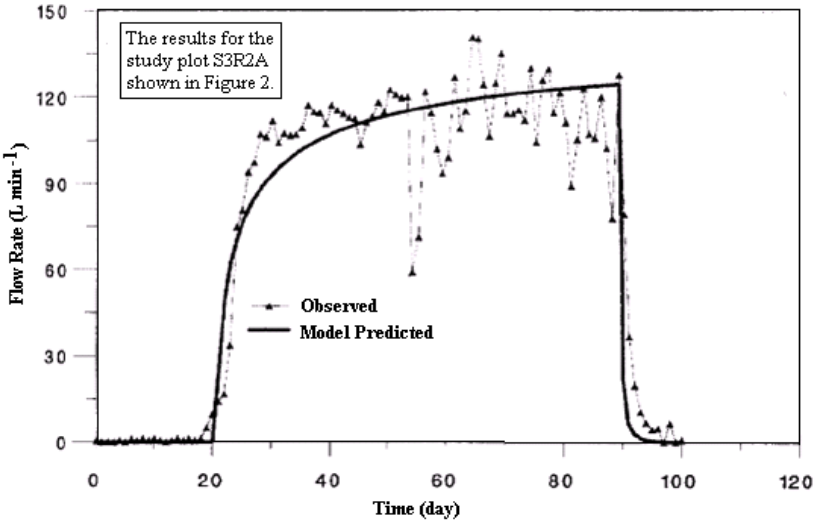

Figure 3-11. Observed versus simulated flow hydrographs at the outlet of the experimental plot S3R2A using the hillslope-scale model. The model is defined by Eqs. (10) and (11). (After Tayfur and Kavvas 1998).

Figure 3-11 shows the runoff simulation results for the experimental plot S3R2A (Figure 3-2; Barfield et al. 1983) using the hillslope-scale averaged flow model as defined by Eqs. (10) and (11). The model input data are summarized in Table 3-1. The results indicate that although the model does not require intensive inputs, it successfully reproduced the observed flow hydrograph. In addition, the model was used to simulate the runoff from a hypothetical hillslope that has a rill density of about 11% (Tayfur and Kavvas, 1994) and the simulation results are shown in Figure 3-12. As expected, the total stream flow was predicted to be mainly from the rills. The interrill sheet flows were predicted to account for less than 5% of the stream flow. This reveals the importance of considering the effects of hills and interills on hydrologic modeling.

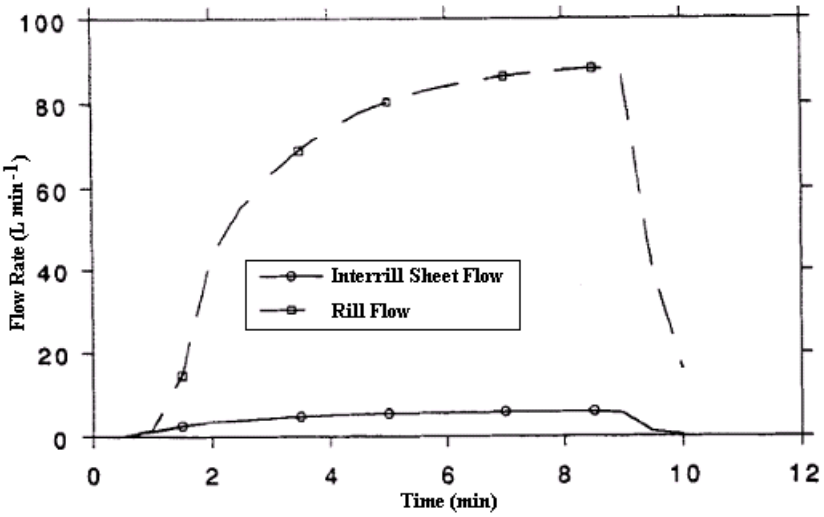

Figure 3-12. Predicted rill flow and interrill sheet flow. (After Tayfur and Kavvas 1994).

MODELING SEDIMENTATION OVER MICROTOPOGRAPHIC SURFACE

Watershed sediment yield is a direct indication of overland erosion rates and quantities of suspended solids that are transported through aquatic systems. Water erosion may incept three sequential processes of detachment, transport, and deposition of soil particles. These processes are controlled by raindrop energy and runoff transport capacity (Foster 1982). Detachment would occur when the erosive force of raindrop or overland flow exceeds the resistance of soil to erosion. Detached particles may then be carried downstream by overland flow. On the other hand, deposition would occur when the sediment load exceeds the runoff transport capacity. Water erosion reduces productivity of cropland and its subsequent sedimentation may degrade water quality because of the agricultural chemicals associated with the fine sediment particles. Further, deposition in water conveyance structures, such as irrigation canals, stream channels, reservoir, estuaries, and harbors, could adversely impact their functionalities (Foster 1982).

Water erosion has been widely studied using laboratory and field experiments (e.g., Kilinc and Richardson 1973; Abrahams et al. 1989; and Govindaraju and Kavvas 1992). Kilinc and Richardson (1973) did extensive rainfall-runoff simulations over slopes of 5.7 to 40% to study the mechanics of soil erosion from overland flow. In addition, Mosley (1974) examined effects of slope and catchment size and slope on rill morphology, discharge, and sediment transport from interrill areas and rills. The author used eight different slopes ranging from 3 to 12%. Further, Moss and Walker (1978), Moss (1979) and Moss et al. (1980; 1982) conducted rainfall-runoff simulations over slopes of 0.1 to 4.2%, measured total sediment concentrations in sheet flow, and examined the formation of rills. Loch and Donnollan (1983a, b) and Loch (1984) measured sediment loadings associated with artificial steady-state

runoff over a tilted slope of 4%. Govindaraju et al. (1992) did rainfall-runoff simulations over steep slopes of weathered granite to assess the erosion from cuttings and/or fillings.

Rainfall-induced overland erosion has also been widely studied using physically-based mathematical models by many researchers (e.g., Negev 1967; Foster and Meyer 1972; and Govindaraju and Kavvas 1991). These studies did not consider the microtopography of overland surfaces, which might oversimplify the aforementioned erosion processes. As advancement, Tayfur (2001) developed a two-dimensional erosion and sediment transport equation and examined typical values of the variables. The equation still approximates the highly irregular microtopography using a smooth surface to avoid complications arising in the numerical solution and extra efforts in obtaining the grid-scale microtopographic data required by the solution. Also, the equation assumes homogeneous soil properties and thus does not allow the roughness and infiltration rate to be varied spatially. Moreover, the equation uses the kinematic wave approximation, which would become invalid when backwater effects are important. As with the previous modeling studies cited above, the equation tends to oversimplify the physical processes of soil erosion. As a further improvement, Tayfur and Singh (2004) incorporated effects of mircotopography on erosion and sediment transport into the equation.

The improved two-dimensional erosion and sediment transport equation (Tayfur, 2001; Tayfur and Singh 2004) can be expressed as:

$$\frac{\partial(hc)}{\partial t} + \frac{\partial}{\partial x}(q_x c) + \frac{\partial}{\partial y}(q_y c) = \frac{1}{\rho_s}\left[\alpha r^{\beta} + \sigma(T_c - q_s)\right] \tag{12}$$

where q_x and q_y are the flow fluxes in the x and y directions, respectively ($L^2\ T^{-1}$); $q_s = \rho_s c\left(q_x^2 + q_y^2\right)^{0.5}$ is the sediment flux ($M\ L^{-1}\ T^{-1}$); $T_c = \eta\left[\gamma h\left(S_x^2 + S_y^2\right)^{0.5} - \delta_s(\gamma_s - \gamma)d\right]^{k_1}$ is the flow transport capacity ($M\ L^{-1}\ T^{-1}$); c is the sediment concentration by volume ($L^3\ L^{-3}$); ρ_s is the sediment particle density ($M\ L^{-3}$); α is the soil detachability coefficient ranging from 0.00012 to 0.0086 kg m^{-2} mm^{-1} (Sharma et al. 1993); β is a constant ranging from 1 to 2; σ is the transfer rate coefficient ranging from 3 to 33 m^{-1} (Foster 1982); η is the soil erodibility coefficient ranging from is 0 to 1.0 (Foster 1982); γ_s is the specific weight of sediment ($M\ L^{-2}\ T^{-2}$); γ is the specific weight of water ($M\ L^{-2}\ T^{-2}$); δ_s is a constant of 0.047 (Gessler 1965); d is the particle diameter (L); and k_1 is an exponent ranging from 1.0 to 2.5 (Foster 1982).

In Eq. (12), αr^{β} describes the soil detachment by raindrop, while $\sigma(T_c - q_s)$ represents the soil detachment and deposition by sheet flow. When $T_c > q_s$, soil particles would be detached. Otherwise, particles will be deposited. This equation is solved conjunctively with Eqs. (1) to (3) to determine the parameters of flow and sediment transport. Eqs (1) to (3) are first solved for the flow variables (i.e., depth, velocity, and flux), which in turn are used in Eq. (12) to determine the parameters for sediment transport. When the water depth and sediment concentration at the upper and lower boundaries are near-zero, they are assumed very small values of 0.00001 m and 0.0001 t m^{-3}. This will eliminate the singularity problem in the numerical solution (Tayfur 2001). The inputs into these equations are summarized in Table 3-2, and the simulation results for the experimental plot S3R2A (Figure 3-2) are shown in Figure 3-13.

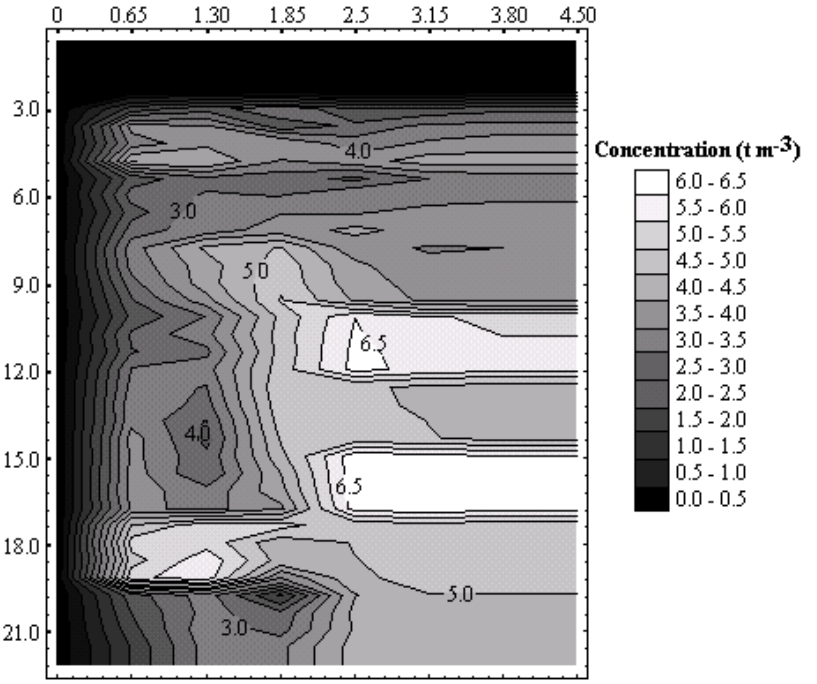

Figure 3-13. Contour map showing the sediment concentration predicted using variable slopes over the experimental plot S3R2A illustrated in Figure 3-2. (After Tayfur and Singh 2004).

Table 3-2. Inputs into Eqs. (1) to (3) and Eq. (12)

Variable	Description	Value
n	Manning's roughness coefficient	0.012
α (kg m^{-2} mm^{-1})	Soil detachability coefficient	0.0022
B	Exponent	1.80
σ (m^{-1})	Transfer rate coefficient	24.0
k_1	Exponent	1.5
H	Soil erodibility coefficient	0.12
r (mm h^{-1})	Rainfall intensity	117
Δt (min)	Rainfall duration	20
i (mm h^{-1})	Constant infiltration rate	7
d (mm)	Particle diameter	1
ρ (kg m^{-3})	Soil bulk density	1500

Although the plot surface was smoothed using a 1.2-m by 0.6-m window (Tayfur and Singh 2004) to stabilize the numerical solution, the predicted sediment concentrations exhibit noticeable spatial variations (Figure 3-13), which reflect the effects of microtopographic slopes. The similar effects can be resulted from heterogeneities of roughness (Figure 3-14) and infiltration rate (Figure 3-15). In this study, the roughness has a mean of 0.0187 and a standard deviation of 0.0066, while the infiltration rate has a mean of 13.89 mm h^{-1} and a standard deviation of 7.95 mm h^{-1}. Compared with those of roughness and local slope, the effects of infiltration rate may be smaller. Nevertheless, the temporal variation of infiltration

rate, as described by the Green-Ampt equation, can greatly influence the predicted sediment loadings (Figure 3-16).

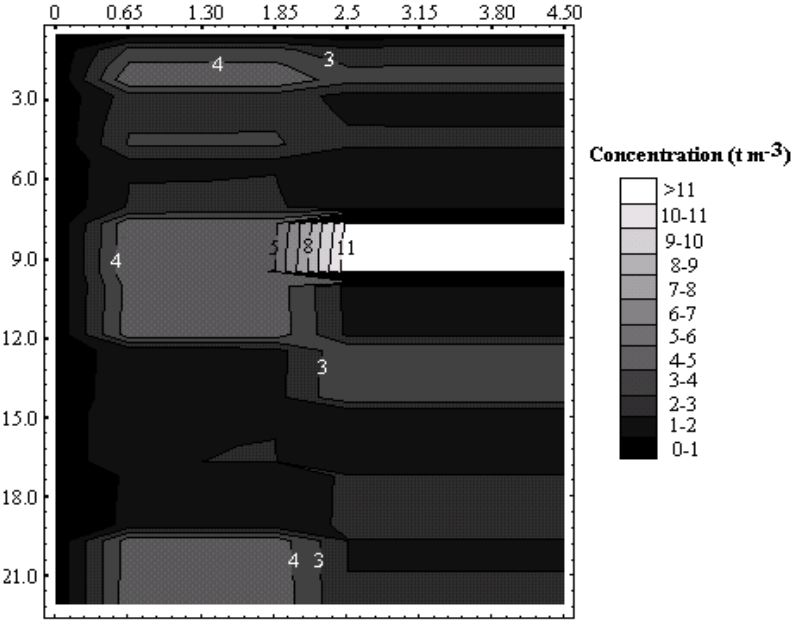

Figure 3-14. Contour map showing the sediment concentration predicted using variable roughness.. (After Tayfur and Singh 2004).

MODELING SEDIMENTATION OVER RILLED SURFACE

As discussed above, microtopographic features such as rills have large effects on hydrologic and erosion processes (Govindaraju and Kavvas 1991; Hairsane and Ross 1992a; Sander et al. 1996; Lisle et al. 1998; Parlange et al. 1999; Hairsane et al. 1999; and Tayfur 2001, 2002). Hairsane and Ross (1992b) developed a theoretical steady-state model for one-dimensional sediment transport from rilled surface. This model assumes that: 1) rills are parallel to each other; 2) rills receive sediment and water fluxes at the transverse direction; 3) rills occur at a fixed frequency of N rills per unit width measured transverse the slope; 4) runoff from an interrill area is directly captured by its adjunct rill and thus the downslope delivery of water solely occurs in the rill; 5) rills have an identical volumetric flow rate; and 6) soils are homogenous. The Water Erosion Prediction Project (WEPP) model also uses a one-dimensional steady-state sediment continuity equation to describe the movement of sediment on rilled surface (Bulygin et al. 2002). In the WEPP model, the interrill sediment delivery is considered to be location independent, and the sediment is conceptualized either to be carried off the hillslope by rill flows or deposited in the rill. These two models are based on equilibrium sediment transport in a rill section and do not consider the transport processes over interrill areas.

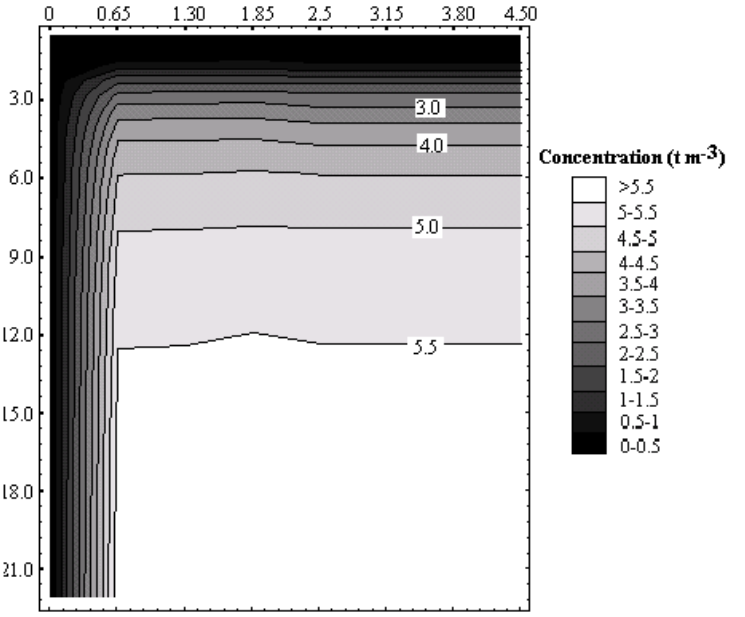

Figure 3-15. Contour map showing the sediment concentration predicted using variable infiltration rate. (After Tayfur and Singh 2004).

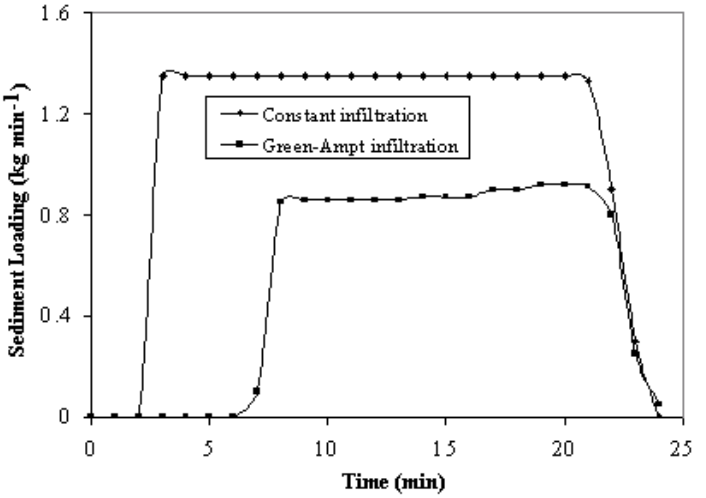

Figure 3-16. The predicted sediment loadings by assuming constant versus temporally variable infiltration rate. (After Tayfur and Singh 2004).

In contrast, Kavvas and Govindaraju (1992) developed an unsteady-state one-dimensional model that considers sheet sediment transport processes over rilled surface. This model takes into account the flow and sediment processes over interrill areas and in rills, but assumes that there is no interaction between these two types of processes. Also, this model does not consider the variability in local microtopography and the lateral sediment inputs from an interrill area into its adjunct rill. To eliminate these limitations and by integrating Eq.

(12) over the length of an interrill area, Tayfur (2007) developed an areal-averaged equation for unsteady-state, non-uniform sheet sediment transport. This two-dimensional equation considers the interactions between rills and interrill areas and the natural variability of surface microtopography. The values for the variables in this equation can be estimated at hillslope scale using digital elevation models. This equation is based on the mass and momentum conservations at hillslope scale and can be expressed as:

$$\frac{\partial\left(\overline{h}_o\overline{c}_o\right)}{\partial t}+\frac{\partial}{\partial x}\left(K_x'\overline{h}_o^{1.5}\overline{c}_o\right)=\frac{1}{\rho_s}\left(\overline{D}_{do}+\overline{D}_{fo}\right)-2.95\frac{K_{yl}}{l}\overline{h}_o^{1.5}\overline{c}_o \tag{13}$$

where $\overline{c}_o$ is the averaged sediment concentration ($L^3\ L^{-3}$) over interrill area; $\overline{h}_o$ is the averaged flow depth (L); $\overline{D}_{do}$ is the averaged soil detachment rate of raindrop on interrill area ($M\ L^{-2}\ T^{-1}$); and $\overline{D}_{fo}$ is the averaged soil detachment/deposition rate of sheet flow over interrill area ($M\ L^{-2}\ T^{-1}$).

The cross-sectional averaged, one-dimensional rill sediment transport equation (Tayfur 2007) can be expressed as:

$$\frac{\partial\left(h_r c_r\right)}{\partial t}+\frac{\partial}{\partial x}\left[K_r R^{0.5} h_r c_r\right]=\frac{1}{\rho_s}D_{fr}+\left(2.95\overline{h}_o^{1.5}\overline{c}_o\right)\left(\frac{K_{yl}}{w_r}\right) \tag{14}$$

$$D_{fr} \;=\; \varphi\left[\eta\left(\tau_r-\tau_c\right)^k-\rho_s c_r K_r R^{0.5} h_r\right] \tag{15}$$

where c_r is the cross-sectional averaged sediment concentration from the rill ($L^3\ L^{-3}$); D_{fr} is the cross-sectional averaged soil detachment/deposition rate by rill flow ($M\ L^{-2}\ T^{-1}$); and $\tau_r=\gamma R S_r$ is the cross-sectional averaged rill shear stress ($M\ L^{-2}$).

Eq (14) neglects the soil detachment due to raindrop from rill section because the raindrop impact is a dominant factor for the detachment of soil particles on interrill areas but in rills detachment and transport by flow are dominant (Foster 1982). The last term on the right hand side of this equation represents the local-scale lateral sediment flux into the rill from its two adjunct interrill areas illustrated in Figure 3-7.

In practice, the numerical solution needs to be simplified and extra efforts to collect very high-resolution data should be minimized. Eqs. (13) and (14) are integrated over the hillslope length (Figs. 3-8 and 3-9) using a local-scale averaging procedure (Tayfur and Kavvas 1998). The areal-averaged equations (Tayfur 2007) are expressed as:

$$\frac{\partial\left(h_o'c_o'\right)}{\partial t}+\frac{2.95}{L_x}\left(K'_{x_{Lx}}h_o'^{1.5}c_o'\right)=\frac{1}{\rho_s}\left(D_{do}'+D_{fo}'\right)-2.95K_{yl}'h_o'^{1.5}c_o' \tag{16}$$

$$\frac{\partial\left(h_r'c_r'\right)}{\partial t}+\left[\frac{2.95K_R h_r'^{1.5}c_r'}{\left(w_{r_{Lx}}+\pi h_r'\right)^{0.5}}\right]=\frac{1}{\rho_s}D_{fr}'+2.95\,h_o'^{1.5}c_o'K_{Y_i}' \tag{17}$$

where c'_o and c'_r are the local-scale areal averaged interrill area and rill sediment concentrations ($L^3\ L^{-3}$), respectively; h'_o and h'_r are the local-scale areal averaged interrill area and rill flow depths (L), respectively; D'_{do} is the local-scale areal averaged soil detachment rate due to raindrop over interrill area ($M\ L^{-2}\ T^{-1}$); and D'_{fo} and D'_{fr} are the local-scale areal averaged soil detachment/deposition rate ($M\ L^{-2}\ T^{-1}$) by sheet and rill flows, respectively; R_{Lx} is the hydraulic radius of the section at the downstream end of a rill; and $K_R = \frac{K_{r_{Lx}} w'^{0.5}_{r_{Lx}}}{L_x}$.

Eqs. (16) and (17) are for modelling the sheet sediment transport over an individual interrill area and the sediment transport in an individual rill. These two equations are statistically averaged over the whole hillslope (Figure 3-10) using a procedure developed by Tayfur and Kavvas (1998). The resulted hillslope-scale sediment transport equations (Tayfur 2007) are expressed as:

$$\frac{\partial\left(h'_o(\bar{r}')c'_o(\bar{r}')\right)}{\partial t} + 1.48\sum_{i=1}^{n}\sum_{j=1}^{n} Cov\left(r_i, r_j\right)\left\{\frac{\partial^2\left[K'_X(\bar{r}')h'^{1.5}_o(\bar{r}')c'_o(\bar{r}')\right]}{\partial r'_i\,\partial r'_j} + \frac{\partial\left[K'_{yl}(\bar{r}')h'^{1.5}_o(\bar{r}')c'_c(\bar{r}')\right]}{\partial r'_i\,\partial r'_j}\right\}$$
$$+ 2.95\left\{K'_X(\bar{r}')h'^{1.5}_o(\bar{r}')c'_o(\bar{r}') + K'_{yl}(\bar{r}')h'^{1.5}_o(\bar{r}')c'_o(\bar{r}')\right\} = \frac{1}{\rho_s}\left[D'_{do}(\bar{r}') + D'_{fo}(\bar{r}')\right] \tag{18}$$

$$\frac{\partial\left(h'_r(\bar{r}')c'_r(\bar{r}')\right)}{\partial t} + 1.48\sum_{i=1}^{n}\sum_{j=1}^{n} Cov\left(r_i, r_j\right)\left\{\frac{\partial^2\left[\frac{K_R(\bar{r}')h'^{1.5}_r(\bar{r}')c'_r(\bar{r}')}{\left(w_{r_{Lx}} + \pi h'_r(\bar{r}')\right)^{0.5}}\right]}{\partial r'_i\ \partial r'_j} - \frac{\partial^2\left[K'_{Y_1}(\bar{r}')h'^{1.5}_o(\bar{r}')c'_r(\bar{r}')\right]}{\partial r'_i\,\partial r'_j} - \frac{\partial^2\left[K'_{Y_2}(\bar{r}')h'^{1.5}_o(\bar{r}')c'_r(\bar{r}')\right]}{\partial r'_i\,\partial r'_j}\right\}$$
$$2.95\left\{\frac{K_R(\bar{r}')h'^{1.5}_r(\bar{r}')c'_r(\bar{r}')}{\left[w_{r_{Lx}} + \pi h'_r(\bar{r}')\right]^{0.5}} - h'^{1.5}_o(\bar{r}')c'_r(\bar{r}')\left[K'_{Y_1}(\bar{r}') + K'_{Y_2}(\bar{r}')\right]\right\} = \frac{1}{\rho_s} D'_{fr}(\bar{r}') \tag{19}$$

where $\bar{r}$ [C_z, S_{ox}, S_{oy}, L_x] is the vector random variable and $\bar{r}'$ is its hillslope-scale mean vector; $h'_o(\bar{r}')$ is the hillslope-scale interrill area sheet flow depth computed by Eq. (10); $c'_o(\bar{r}')$ is the hillslope-scale interrill area sediment concentration; $D'_{do}(\bar{r}')$ is the hillslope-scale soil detachment rate by raindrop over interrill area; $D'_{fo}(\bar{r}')$ is the hillslope-scale soil detachment/deposition rate by sheet flow over interrill area; $h'_r(\bar{r}')$ is the hillslope-scale rill flow depth computed by Eq. (11); $c'_r(\bar{r}')$ is the hillslope-scale rill sediment concentration; $D'_{fr}(\bar{r}')$ is the hillslope-scale rill soil detachment/deposition rate; and $K'_X = \frac{K'_{x_{Lx}}}{L_x}$.

Eqs. (10) and (11) are conjunctively solved first to determine the hillslope-scale averaged flow depths and fluxes over interrill areas and in rills. The results are taken as inputs of Eqs. (18) and (19), which in turn are conjunctively solved for each time step. Eq. (18) is solved to calculate the hillslope-scale averaged sediment loading into rills and Eq. (19) is then solved to

calculate the hillslope-scale averaged sediment loading from the rills into the stream located at the bottom end of the hillslope. In order to determine the total sediment loading from a hillslope into the stream, the probability of rill occurrence λ over the hillslope needs to be estimated using a high-resolution (e.g., 10-m) DEM (Govindaraju et al. 1992; Govindaraju and Kavvas 1992; and Kavvas and Govindaraju 1992). The hillslope-scale averaged rill sediment loading into the stream is multiplied by λ, and the hillslope-scale averaged interrill-area sediment loading into the stream is multiplied by (1-λ). These products are then summed up to get the total sediment loading from the hillslope into the adjunct stream.

The geometrics of rills and interrill areas can be determined using the DEM. The solution of Eqs. (18) and (19) requires that the width of a hillslope be greater than the ergodic length scale (i.e., 6 to 8 m) but be smaller than the terrain length scale. Also, the solution assumes that the geometry of a rill is fixed throughout a simulation period, but each rill's geometry may be different from the others'. This assumption is usually valid for rainstorms with a moderate or smaller intensity.

Table 3-3. Geometrics of the rills over the experimental hillslope in northern California[1]

Distance (m)	Expected Spatial Rill Density (%)	Mean Rill Depth (cm)	Mean Rill Width (cm)
9.0	0.1	7.0	10.0
10.5	0.2	8.0	14.0
12.0	0.2	9.0	16.0
13.5	25.0	9.5	19.0
15.0	28.0	11.0	22.0
16.5	0.3	11.5	22.5
18.0	33.0	12.0	23.5
19.5	0.4	12.0	24.0
21.0	38.0	13.0	25.0
22.5	0.4	13.0	24.5
24.0	38.0	13.0	25.5

[1] The data are from Govindaraju et al. (1992).

The solution was used to simulate the flows and sediment loadings from a cut bare hillslope located near Buckhorn Summit in Northern California in the United States of America (USA). The simulation results were compared with the corresponding observed values of the rainfall-runoff experiment conducted by Govindaraju et al. (1992) (Figs. 3-17 and 3-18). The hillslope has an average slope of about 67%. The lower portion of the hillslope, which is about 15 m long and 10 m wide, was subjected to intense rainfall of 152 mm h^{-1} for a duration period of 10 minutes. The sediment laden flow was collected at the downstream along the width of the slope after steady state had been achieved. The sediment loading was measured using a Parshall flume. The rill geometrics were surveyed using a tape measure and a ruler at 11 locations along the slope spaced at 1.5 m (Table 3-3). Govindaraju et al. (1992) determined that the hillslope has a Chezy roughness coefficient of $C_z = 16.6\ m^{0.5}$

s^{-1}. A laboratory test using 23 soil samples indicated that the hillslope has a saturated hydraulic conductivity of K_s = 37.8 mm h^{-1}. The infiltration rate was estimated using the Horton's formula with a rate constant of k = 0.0014 s^{-1} and an initial infiltration rate of f_o = 127 mm h^{-1}. The sediment density was measured to be 2662 kg m^{-3} (Govindaraju et al. 1992).

The solution successfully predicted both the flows (Figure 3-17) and the sediment loadings (Figure 3-18). The good predicted was further indicated by the low absolute errors of 11.07 L min^{-1} for flows and 0.382 kg s^{-1} for sediment loadings. Thus, the solution is judged to be capable in simulating the flow and sedimentation processes over rilled hillslopes.

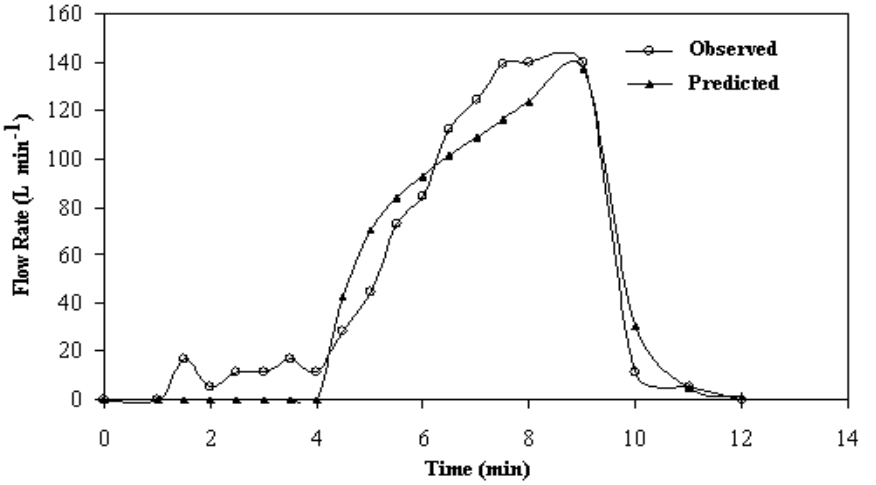

Figure 3-17. The observed versus predicted flows from the experimental hillslope near Buckhorn Summit in northern California. (After Tayfur 2007).

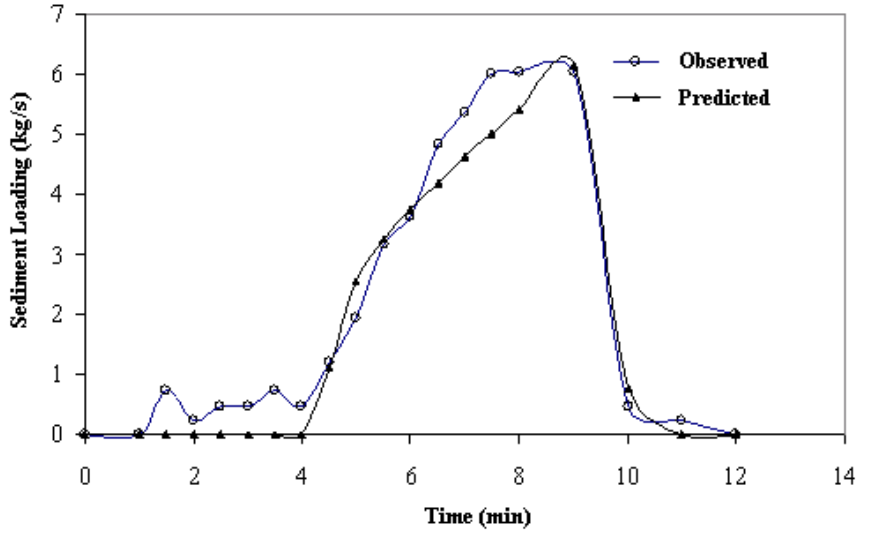

Figure 3-18. The observed versus predicted sediment loadings from the experimental hillslope near Buckhorn Summit in northern California. (After Tayfur 2007).

CONCLUSIONS

Understanding the physical processes of flow and sedimentation at hillsope scale is essential for watershed modeling. This chapter reviews the improved modeling approaches that enable considering the important effects of microtopographic features (e.g., local slope, rill, interrill, and variable roughness) on the processes. The results indicate that although the hillslope-scale areal averaged equations use easily-available data, they did very good jobs in predicting the flows and sediment loadings in the experiment plot S3R2A and the experiment hillslope in northern California in USA. The improved modeling approaches are expected to increase the analysis accuracy in comparison with the conventional methods that neglect microtopographic features.

ACKNOWLEDGMENTS

The author is grateful to B.J. Barfield and D.E. Storm of the Department of Agricultural Engineering, College of Agriculture, University of Kentucky, for providing observed hydrographs and three-dimensional picture of the experiment plot S3R2A.

REFERENCES

Abrahams, A.D. and Parsons, A.J. (1990). Determining the mean depth of overland flow in field studies of flow hydraulics. *Water Resour. Res.*, 26, 501-503.

Abrahams, A.D., Parsons, A.J. and Luk, S.-H. (1989). Distribution of depth of overland flow on desert hillslopes and its implication for modeling soil erosion. *J. Hydrology*, 106, 177-184.

Barfield, B.J., Barnhisel, R.I., Powell, J.L., Hirschi, M.C. and Moore, I.D. (1983). Erodibilities and eroded size distribution of Western Kentucky mine spoil and reconstructed topsoil. *Institute for Mining and Minerals Research Final Report,* Univ. of Kentucky, Lexigton, KY.

Bulygin, S.Y., Nearing, M.A. and Achasov, A.B. (2002). Parameters of interrill erodibility in the WEPP model. *Eurasian Soil Sci*, 35(11), 1237-1242.

Emmett, W.W. (1978). Overland Flow. *In: M.J. Kirkby (ed.) Hillslope Hydrology*, John Wiley and Sons, New York, N.Y., 145-176.

Engman, E.T. and Gurney, R.J. (1991). Remote sensing in hydrology, Chapman and Hall, London, UK.

Foster, G.R. (1982). Modelling the erosion process. *In : C.T. Haan, H.P. Johnson and D.L. Brakensiek (Editors), Hydrologic modelling of small watersheds'. ASAE*, 295-380.

Foster, G.R. and Meyer, L.D. (1972). A closed-form soil erosion equation for upland areas. *Sedimentation Symposium to Honor Prof. H.A. Einstein*, H.W. Shen ed., Fort Collins, Colorado, 12.1-12.9.

Gessler, J. (1965). The beginning of bedload movement of mixtures investigated as natural armoring in channels. E.A. Prych, translator, W.M. Keck Laboratory of Hydraulics and Water Research, CIT, Pasedana, California.

Govindaraju, R.S. and Kavvas, M.L. (1991). Modelling the erosion process over steep slopes: approximate analytical solutions. *J. of Hydrology*, 127, 279-305.

Govindaraju, R.S. and Kavvas, M.L. (1992). Characterization of the rill geometry over straight hillslopes through spatial scales. *J. Hydrology*, 130, 339-365.

Govindaraju, R.S., Jones, S.E. and Kavvas, M.L. (1988), On the Diffusion Wave Model for Overland Flow, 1, Solution for Steep Slopes. *Water Resources Research*, 24(5), 734-744.

Govindaraju, R.S., Kavvas, M.L., Tayfur, G. and Krone, R.B. (1992). Erosion control of decomposed granite at Buckhorn Summit. *Final Report*. California Department of Transportation.

Hairsane, P.B. and Rose, C.W. (1992a). Modelling water erosion due to overland flow using physical principles, 1. sheet flow. *Water Resour. Res*., 28(1), 237-243.

Hairsane, P.B. and Rose, C.W. (1992b). Modelling water erosion due to overland flow using physical principles, 2. rill flow. *Water Resour. Res*., 28(1), 244-250.

Hairsane, P.B., Sander, G.C., Rose, C.W., Parlange, J.-Y, Hogarth, W.L., Lisle, I. and Rouhipour, H. (1999). Unsteady soil erosion due to rainfall impact: a model of sediment sorting on the hillslope. *J. Hydrology,* 220, 115-128.

Kavvas, M.L. and Govindaraju, R.S. (1992). Hydrodynamic averaging of overland flow and soil erosion over rilled hillslopes. *Erosion, Debris Flows and Environment in Mountain Regions, Proceedings of the Chengdu Symposium,* IAHS Publ: 209.

Kilinc, M. and Richardson, E.V. (1973). Mechanics of soil erosion from overland flow generated by simulated rainfall. *Hydrology Papers, Colorado State University*, Fort Collins, Paper 63.

Li, R.M., Ponce, V.M. and Simons, D.B. (1980). Modeling rill density. *J. Irrig. and Drain. Div.*, ASCE, 106(1), 63-67.

Lisle, I.G., Rose, C.W., Hogarth, W.L., Hairsine, P.B., Sander, G.C. and Parlange, J.-Y. (1998). Stochastic sediment transport in soil erosion. *J. Hydrology*, 204(1-4), 217-230.

Loch, R.J. (1984). Field rainfall simulator studies on two clay soils of the Darling Downs, Queensland, III, An evaluation of current methods of deriving soil erodibilities (K factors). *Aust. J. Soil Res*., 22, 401-412.

Loch, R.J. and Donnollan, T.E. (1983a). Field rainfall simulator studies on two clay soils of the Darling Downs, Queensland, I, The effects of plot length and tillage orientation on erosion processes and runoff erosion rates. *Aust. J. Soil Res*., 21, 33-46.

Loch, R.J. and Donnollan, T.E. (1983b). Field rainfall simulator studies on two clay soils of the Darling Downs, Queensland, II, Aggregate breakdown, sediment properties and soil erodibility. *Aust. J. Soil Res*., 21, 47-58.

Mankin, K.R., Koelliker, J.K. and Kalita, P.K. (1999). Watershed and lake water quality assessment: An integrated modeling approach. *J. Am. Water Resour. Assoc*., 35(5), 1069-1088.

Meyer, L.D., Foster, G.R. and Romkens, M.J.M. (1975). Source of soil eroded from upland slopes. *Proc. 1972 Sediment Yield Workshop, U.S. Dept. Agric. Sediment Lab.,* Oxford, Mississippi, ARS-S-40, USDA, 177-189.

Moore, I.D. and Foster, G.R. (1989). Hydraulics and Overland Flow, *Process studies in hillslope hydrology,* John Wiley&Sons, Sussex, England, UK, 1-34.

Mosley, M.P. (1974). Experimental study of rill erosion. *Trans. Am. Soc. Agric. Eng*., 17, 909-913.

Moss, A.J. (1979). Thin flow transportation of solids in arid and non-arid areas: A comparison of processes. IAHS-AISH Publ., 128, 435-445.

Moss, A.J., and Walker, P.H. (1978). Particle transport by continental water flows in relation to erosion, deposition, soil and human activities. *Sediment,* Geology, 20(2), 81-139.

Moss, A.J., Green, P. and Hutka, J. (1982). Small channels: Their experimental formation, nature and significance. *Earth Surf. Process. Landforms*, 7, 401-415.

Moss, A.J., Walker, P.H., and Hutka, J. (1980). Movement of loose, sandy detritus by shaloow water flows: An experimental study. *Sediment. Geol.,* 25, 43-66.

Negev, N. (1967). A sediment model on a digital computer. Tech. Rep. No. 76, Stanford University, California, 109 pp.

Parlange, J.-Y., Hogarth, W.L., Rose, C.W., Sander, G.C., Hairsine, P. and Lisle, I. (1999). Addendum to unsteady soil erosion model. *J. Hydrology*, 217(1-2), 149-156.

Rudra, R.P., Dickinson, W.T., Abedini, N.J. and Wall, G.J. (1999). A multi-tier approach for agricultural watershed management. *J. Am. Water Resour. Assoc*., 35(5), 1059-1070.

Sander, G.C., Hairsine, P.B., Rose, C.W., Cassidy, D., Parlange, J.-Y., Hogarth, W.L. and Lisle, I.G. (1996). Unsteady soil erosion model, analytical solutions and comparison with experimental results. *J. Hydrology*, 178(1-4), 351-367.

Sharma, P.P., Gupta, S.C. and Foster, G.R. (1993). Predicting soil detachment by raindrops. *Soil Sci. Soc. Am. Journal*, 57, 674-680.

Singh, V.P. and Woolhiser, D.D. (2002). Mathematical modeling of watershed hydrology. *J. Hydrologic Engrg*. ASCE, 7(4), 270-292.

Tayfur, G. (2001). Modelling two dimensional erosion process over infiltrating surfaces. *J. Hydrologic Engrg,* ASCE, 6(3), 259-262.

Tayfur, G. (2002). Applicability of sediment transport capacity models for non-steady state erosion from steep slopes." *J. Hydrologic Engrg,* ASCE, 7(3), 252-259.

Tayfur, G. (2007). Modeling sediment transport from bare rilled hillslopes by areally averaged transport equations. *Catena*, 70, 25-38.

Tayfur, G. and Kavvas, M.L. (1998). "Areal averaged overland flow equations at hillslope scale." *Hydrological Sciences J.,* IAHS, 43(3):361-378.

Tayfur, G. and Singh, V.P. (2004). Numerical model for sediment transport over non-planar, non-homogeneous surfaces. *J. Hydrologic Engrg*. ASCE , 9(1), 35-41.

Tayfur, G., and Kavvas, M.L. (1994). Spatially averaged conservation equations for interacting rill-interrill area overland flows . *J. Hydraulic Engrg,* ASCE, 120(12), 1426-1448.

Tayfur, G., Kavvas, M.L., Govindaraju, R.S., and Storm, D.E. (1993). Applicability of St.Venant equations for two-dimensional overland flows over rough infiltrating surfaces. *J. Hydraulic Engrg*, ASCE, 119(1), 51-63.

Wurbs, R.A. (1998). Dissemination of generalized water resources models in the United States. *Water Int.,* 23, 190-198.

Zhang, W. and Cundy, T.W. (1989). Modeling of two dimensional overland flow. *Water Resources Research,* 25(9), 2019-2035.